Theory of Topological Spin Hall Effect in Antiferromagnetic Skyrmions: Impact on Current-induced Motion

C. A. Akosa[1,2],* O. A. Tretiakov[3], G. Tatara[1,4], and A. Manchon[2]

[1]*RIKEN Center for Emergent Matter Science (CEMS), 2-1 Hirosawa, Wako, Saitama 351-0198, Japan*

[2]*King Abdullah University of Science and Technology (KAUST), Physical Science and Engineering (PSE) Division, Thuwal 23955-6900, Saudi Arabia*

[3]*Institute for Materials Research, Tohoku University, Sendai 980-8577, Japan and*

[4]*RIKEN Cluster for Pioneering Research (CPR), 2-1 Hirosawa, Wako, Saitama, 351-0198 Japan*

(Dated: August 2, 2018)

* collins.akosa@riken.jp

I. EMERGENT ELECTROMAGNETISM FOR ANTIFERROMAGNETS

Consider an antiferromagnet with equivalent sublattices a and b. In the coupled sublattice-spin space $(|a\rangle, |b\rangle) \otimes (|\uparrow\rangle, |\downarrow\rangle)$, the Hamiltonian can be written as

$$\mathcal{H} = (\epsilon\hat{\mathbb{I}}_2 + \gamma_k\hat{\tau}_x) \otimes \hat{\mathbb{I}}_2 - J(\hat{\tau}_z \otimes \mathbf{n} + \hat{\mathbb{I}}_2 \otimes \mathbf{m}) \cdot \hat{\boldsymbol{\sigma}}, \tag{1}$$

where J is the exchange coupling, $\hat{\boldsymbol{\sigma}}$ is the spin of the electron, t is the nearest-neighbor hopping, ϵ_i and $\hat{c}_i^\dagger$ ($\hat{c}_i$) are the onsite energy, and the spinor creation (annihilation) operator of site i, respectively. $\gamma_k = -2t(\cos k_x a_0 + \cos k_y a_0)$, a_0 is the lattice constant, $\hat{\mathbb{I}}_2$ is the 2×2 identity matrix, $\mathbf{n} = \frac{1}{2}(\mathbf{m}^a - \mathbf{m}^b)$ and $\mathbf{m} = \frac{1}{2}(\mathbf{m}^a + \mathbf{m}^b)$ are unit vectors in the direction of the Néel vector and the total magnetization, respectively. $\hat{\boldsymbol{\tau}}$ and $\hat{\boldsymbol{\sigma}}$ are the Pauli matrices of the sublattice and spin subspaces, respectively. For a smooth and slowing varying $\mathbf{n}(\mathbf{r}, t)$, the eigenvalues and eigenstates corresponding to Eq. (1) are given by

$$\epsilon_s^\eta(k) = s\sqrt{\gamma_k^2 + J^2} \tag{2}$$

and

$$\Psi_s^{\eta,\sigma} = \sum_\eta s\sqrt{\frac{1 + s\eta\sigma P_k}{2}}|\eta\rangle \otimes |\sigma\rangle, \tag{3}$$

respectively, where $s = +1(-1)$ represents the doubly generate bands above (below) the band gap and in the rest of this paper, wet set $s = +1$. $P_k = J/\sqrt{\gamma_k^2 + J^2}$ is the polarization of the local density of states projected on the η-sublattice and $\eta = +(-)1$ for the $(a)b$-sublattice [1, 2]. The third term on the right hand side of Eq. (1) can be diagonalized via a unitary acting *only* on the spin-subspace, $\mathcal{U} = e^{-i\frac{\theta}{2}\hat{\boldsymbol{\sigma}}\cdot\mathbf{e}_\phi}$, where $\mathbf{e}_\phi = \mathbf{z} \times \mathbf{n}/|\mathbf{z} \times \mathbf{n}|$ [5–7], to obtain

$$\tilde{\mathcal{H}} \approx \frac{1}{2m}(\hat{\mathbf{p}} + e\hat{\mathbf{A}})^2\hat{\tau}_x \otimes \hat{\mathbb{I}}_2 - J\hat{\tau}_z \otimes \hat{\sigma}_z - e\hat{\mathbb{I}}_2 \otimes \hat{A}_0. \tag{4}$$

$\hat{\mathbf{A}} = -(\hbar/2e)\big([\mathbf{n}\times\partial_i\mathbf{n}]\cdot\hat{\boldsymbol{\sigma}}^{\eta}\big)\mathbf{e}_i$ and $\hat{A}_0 = (\hbar/2e)\big([\mathbf{n}\times\partial_t\mathbf{n}]\cdot\hat{\boldsymbol{\sigma}}^{\eta}\big)\mathbf{z}$ are the vector and scalar potentials, respectively. $\hat{\boldsymbol{\sigma}}^{\eta} = \frac{1}{2}(\hat{\mathbb{I}}_2 + \eta\hat{\tau}_z)\otimes\hat{\boldsymbol{\sigma}}$ is the spinor operator, with expected value with respect to the eigenstates given in Eq. (3) given as

$$\langle|\hat{\boldsymbol{\sigma}}^{\eta}|\rangle = \sigma P^{\eta}_{\sigma}, \tag{5}$$

where $P^{\eta}_{\sigma} = \frac{1}{2}(1+\eta\sigma P_k)$, $\sigma = +(-)1$ for $\uparrow$ ($\downarrow$) spin. As a result, the spin-dependent carriers feel an emerging electromagnetic field for the η-sublattice given by,

$$\mathbf{E}^{\eta,\sigma}_{\rm em} = (\sigma\hbar/2e)P^{\eta}_{\sigma}\mathcal{N}_{t,i}(\boldsymbol{r})\mathbf{e}_i \tag{6a}$$

$$\mathbf{B}^{\eta,\sigma}_{\rm em} = -(\sigma\hbar/2e)P^{\eta}_{\sigma}\mathcal{N}_{x,y}(\boldsymbol{r})\mathbf{z} \tag{6b}$$

where $\mathcal{N}_{\mu,\nu}(\boldsymbol{r}) = (\partial_\mu\boldsymbol{n}\times\partial_\nu\mathbf{n})\cdot\mathbf{n}$, with $\nu,\mu\in(t,x,y)$. Observe that close to the van Hove singularity or as J goes to infinity, $P_k = 1$, we have $\big(\ P^a_{\uparrow}=1\ ,\ P^a_{\downarrow}=0\ \big)$ and $\big(\ P^b_{\uparrow}=0\ ,\ P^b_{\downarrow}=1\ \big)$ i.e.

$$\mathbf{E}^{a,\uparrow}_{\rm em} = (\hbar/2e)\mathcal{N}_{t,i}(\boldsymbol{r})\mathbf{e}_i \quad , \quad \mathbf{E}^{a,\downarrow}_{\rm em} = 0 \tag{7a}$$

$$\mathbf{B}^{a,\uparrow}_{\rm em} = -(\hbar/2e)\mathcal{N}_{x,y}(\boldsymbol{r})\mathbf{z} \quad , \quad \mathbf{B}^{a,\downarrow}_{\rm em} = 0 \tag{7b}$$

and

$$\mathbf{E}^{b,\uparrow}_{\rm em} = 0 \quad , \quad \mathbf{E}^{a,\downarrow}_{\rm em} = -(\hbar/2e)\mathcal{N}_{t,i}(\boldsymbol{r})\mathbf{e}_i \tag{8a}$$

$$\mathbf{B}^{b,\uparrow}_{\rm em} = 0 \quad , \quad \mathbf{B}^{a,\downarrow}_{\rm em} = (\hbar/2e)\mathcal{N}_{x,y}(\boldsymbol{r})\mathbf{z}, \tag{8b}$$

respectively as two independent ferromagnets. Under the action of an external electric field applied along the x-axis (i.e. $\mathbf{E} = E\mathbf{x}$), the resulting spin- and sub-lattice-dependent local carrier current density is given by

$$\mathbf{j}^{\eta,\sigma}_{\rm cc} = \sigma^{\eta,\sigma}_0\mathbf{E} + \sigma^{\eta,\sigma}_0\mathbf{E}^{\eta,\sigma}_{\rm em} + \sigma^{\eta,\sigma}_{\rm H}\mathbf{E}\times\mathbf{B}^{\eta,\sigma}_{\rm em}, \tag{9}$$

where $\sigma^{\eta,\sigma}_0$ and $\sigma^{\eta,\sigma}_{\rm H}$ are proportional to the σ-contribution to the normal and Hall conductivity, respectively. Our considerations are based on an AFM-Sk with radius

r_0, embedded in a large system of radius $R \gg r_0$ moving rigidly with velocity $\mathbf{v}$ (i.e. $\partial_t \mathbf{n} = -(\mathbf{v}\cdot\nabla)\mathbf{n}$). Without loss of generality, we chose the profile defined in spherical coordinates as $\mathbf{n} = (\cos\Phi\sin\theta, \sin\Phi\sin\theta, \cos\theta)$, where $\cos\theta = p(r_0^2 - r^2)/(r_0^2 + r^2)$ and $\Phi = qArg(x+iy) + c\pi/2$ are the polar and azimuthal angles, respectively. The constants p, q and c which takes values ± 1, defines the polarization, vorticity and the chirality, respectively.

Before we proceed, we note that the spin transport in AFMs involves inter-sub-lattice mixing, therefore, one is faced with the tedious task of keeping track of the sub-lattice indices. However, for equivalent sub-lattices;

- $\sigma^a_{0(\mathrm{H})} = \sigma^b_{0(\mathrm{H})} \equiv \frac{1}{2}\sigma_{0(\mathrm{H})}$ and
- $\mathcal{P}^a_{0(\mathrm{H})} = -\mathcal{P}^b_{0(\mathrm{H})} \equiv \mathcal{P}_{0(\mathrm{H})}$ (i.e. the overall current polarization is zero),

where $\sigma_{0(\mathrm{H})}$ and $\mathcal{P}_{0(\mathrm{H})}$ are the ordinary (Hall) conductivity and current polarization, respectively while $\sigma^\eta_{0(\mathrm{H})}$ and $\mathcal{P}^\eta_{0(\mathrm{H})}$ are their respective projections on the η-sub-lattice. Therefore, to make our analysis trackable and easy to follow, we define effective polarizations $\bar{P}^\eta_{0(\mathrm{H})}$ and $\tilde{P}^\eta_{0(\mathrm{H})}$ which are odd and even under sub-lattice exchange, given respectively as

$$\bar{P}^\eta_{0(\mathrm{H})} = (\mathcal{P}^\eta_{0(\mathrm{H})} + \eta P_k)/2 = \eta(\mathcal{P}_{0(\mathrm{H})} + J/\epsilon_{\mathrm{F}})/2 \equiv \eta\bar{P}_{0(\mathrm{H})} \tag{10a}$$

and

$$\tilde{P}^\eta_{0(\mathrm{H})} = (1 + \eta P_k \mathcal{P}^\eta_{0(\mathrm{H})})/2 = (1 + \mathcal{P}_{0(\mathrm{H})} J/\epsilon_{\mathrm{F}})/2 \equiv \tilde{P}_{0(\mathrm{H})}, \tag{10b}$$

where ϵ_{F} is the Fermi energy. Putting all these together, the local charge and spin current densities projected on the sub-lattices are calculated from Eq. (9) as $\boldsymbol{j}^\eta_e = \left(\boldsymbol{j}^{\eta,\uparrow}_{cc} + \boldsymbol{j}^{\eta,\downarrow}_{cc}\right)$ and $\boldsymbol{j}^\eta_s = \mathbf{n} \otimes \frac{\hbar}{2e}\left(\boldsymbol{j}^{\eta,\uparrow}_{cc} - \boldsymbol{j}^{\eta,\downarrow}_{cc}\right)$, respectively to obtain

$$\boldsymbol{j}^\eta_e = \frac{1}{2}\Big(\sigma_0\mathbf{x} + \eta\sigma_{xy}(\boldsymbol{r})\mathbf{y}\Big)E + \frac{\eta\hbar\bar{P}_0\sigma_0}{4}\mathcal{N}_{x,y}(\boldsymbol{r})(\mathbf{v}\times\mathbf{z}), \tag{11a}$$

$$\boldsymbol{j}^\eta_s = \mathbf{n}\otimes\frac{1}{2}\Big(\eta\mathbf{x} - pq\beta_{\mathrm{T}}(\boldsymbol{r})\mathbf{y}\Big)b_{\mathrm{J}} + \frac{pq}{2}\alpha_{\mathrm{T}}(\boldsymbol{r})\mathbf{n}\otimes(\mathbf{v}\times\mathbf{z}), \tag{11b}$$

where $b_{\rm J} = \gamma\hbar\mathcal{P}_0\sigma_0 E/2eM_{\rm s}$, M_s being the saturation magnetization, $\sigma_{xy}(\boldsymbol{r}) = (\hbar/2e)\bar{P}_{\rm H}\sigma_{\rm H}\mathcal{N}_{x,y}(\boldsymbol{r})$ is the non-local steady state transverse conductivity while $\alpha_{\rm T}(\boldsymbol{r}) = pq\lambda_{\rm E}^2\mathcal{N}_{x,y}(\boldsymbol{r})$ and $\beta_{\rm T}(\boldsymbol{r}) = pq\lambda_{\rm H}^2\mathcal{N}_{x,y}(\boldsymbol{r})$ are dimensionless constants which as we shall see later, are non-local contributions to the Gilbert damping and non-adiabatic torque, respectively. Finally, the constants $\lambda_{\rm H}^2 = \hbar\tilde{P}_{\rm H}\sigma_{\rm H}/(2e\mathcal{P}_0\sigma_0^{\eta})$ and $\lambda_{\rm E}^2 = \gamma\hbar^2\tilde{P}_0\sigma_0/(4e^2M_{\rm s})$ have dimensions of length squared are length scales associated with the emergent magnetic and electric fields, respectively [8]. The spin torque corresponding to the spin current density in Eq. (11b) is computed using the relation

$$\boldsymbol{\tau}_{\rm T}^{\eta} = -\boldsymbol{\nabla}\cdot\mathbf{j}_s^{\eta}, \tag{12}$$

to obtain

$$\boldsymbol{\tau}_{\rm T}^{\eta} = -\frac{\eta}{2}b_{\rm J}\partial_x\mathbf{n} + \frac{pq}{2}\beta_{\rm T}(\boldsymbol{r})b_{\rm J}\partial_y\mathbf{n} - \frac{pq}{2}\alpha_{\rm T}(\boldsymbol{r})\big(v_y\partial_x\mathbf{n} - v_x\partial_y\mathbf{n}\big). \tag{13}$$

Furthermore, using the fact that

$$\partial_y\mathbf{n} = pq\mathbf{n}\times\partial_x\mathbf{n} \quad \text{and} \quad \mathbf{n}\times\partial_t\mathbf{n} = pq\big(v_y\partial_x\mathbf{n} - v_x\partial_y\mathbf{n}\big), \tag{14}$$

Eq. (15) can be re-written in the form

$$\boldsymbol{\tau}_{\rm T}^{\eta} = -\frac{\eta}{2}b_{\rm J}\partial_x\mathbf{n} + \frac{1}{2}\beta_{\rm T}(\boldsymbol{r})b_{\rm J}\mathbf{n}\times\partial_x\mathbf{n} - \frac{1}{2}\alpha_{\rm T}(\boldsymbol{r})\mathbf{n}\times\partial_t\mathbf{n}. \tag{15}$$

Finally, the total spin transfer torque on the magnetization is calculated as the algebraic sum of the sub-lattice resolved torques (i.e. $\boldsymbol{\tau}_{\rm T} = \boldsymbol{\tau}_{\rm T}^{a} + \boldsymbol{\tau}_{\rm T}^{b}$) to obtain

$$\boldsymbol{\tau}_{\rm T} = \beta_{\rm T}(\boldsymbol{r})b_{\rm J}\mathbf{n}\times\partial_x\mathbf{n} - \alpha_{\rm T}(\boldsymbol{r})\mathbf{n}\times\partial_t\mathbf{n}. \tag{16}$$

For a more general consideration, we include non-adiabatic effects arising from, for example spin relaxation via a constant non-adiabaticity parameter β and the Gilbert damping torque with constant damping constant α, such that the total spin transfer torque is given as

$$\boldsymbol{\tau} = -\boldsymbol{\tau}_{\rm T} - \beta b_{\rm J}\mathbf{n}\times\partial_x\mathbf{n} + \alpha\mathbf{n}\times\partial_t\mathbf{n} \tag{17}$$

Or equivalently, we have

$$\boldsymbol{\tau} = \alpha_{\text{eff}}(\mathbf{r})\mathbf{n} \times \partial_t \mathbf{n} - \beta_{\text{eff}}(\mathbf{r}) b_{\text{J}} \mathbf{n} \times \partial_x \mathbf{n}, \tag{18}$$

where

$$\beta_{\text{eff}}(\mathbf{r}) = \beta + \beta_{\text{T}}(\boldsymbol{r}) \tag{19a}$$

and

$$\alpha_{\text{eff}}(\mathbf{r}) = \alpha + \alpha_{\text{T}}(\boldsymbol{r}). \tag{19b}$$

To arrive at Eq. (18), we have used the fact that η change sign on different sub-lattice and therefore, the adiabatic component of the torque in Eq. (15) vanishes upon taking the summation on both sub-lattice. The effective damping and non-adiabaticity parameters are calculated as

$$\alpha_{\text{eff}}(\boldsymbol{r}) = \alpha + pq\lambda_{\text{E}}^2 \mathcal{N}_{x,y}(\boldsymbol{r}) \tag{20a}$$

and

$$\beta_{\text{eff}}(\boldsymbol{r}) = \beta + pq\lambda_{\text{H}}^2 \mathcal{N}_{x,y}(\boldsymbol{r}), \tag{20b}$$

respectively.

To extract the scaling laws that governs the adiabatic and non-adiabatic spin torque, we note that since the torque $\boldsymbol{\tau}$ can always be decomposed into its adiabatic τ_{ad} and non-adiabatic τ_{na} components as

$$\boldsymbol{\tau} = \tau_{\text{ad}} \partial_x \mathbf{n} + \tau_{\text{na}} \mathbf{n} \times \partial_x \mathbf{n}, \tag{21}$$

the projection of the Eq. (21) on $\partial_x \mathbf{n}$ ($\mathbf{n} \times \partial_x \mathbf{n}$) and integrated over space yields the adiabatic (non-adiabatic) component of the torque. In other words,

$$\tau_{\text{ad}} = \frac{\int_V \big(\boldsymbol{\tau} \cdot \partial_x \mathbf{n}\big) \mathrm{d}^3\mathbf{r}}{\int_V \big(\partial_x \mathbf{n} \cdot \partial_x \mathbf{n}\big) \mathrm{d}^3\mathbf{r}} \tag{22a}$$

and

$$\tau_{\rm na} = \frac{\int_V \big(\boldsymbol{\tau}\cdot(\mathbf{n}\times\partial_x\mathbf{n})\big)\mathrm{d}^3\mathbf{r}}{\int_V \big((\mathbf{n}\times\partial_x\mathbf{n})\cdot(\mathbf{n}\times\partial_x\mathbf{n})\big)\mathrm{d}^3\mathbf{r}}. \tag{22b}$$

Therefore, the adiabatic ($\tau_{\rm ad}$) and non-adiabatic ($\tau_{\rm na}$) components of the torques can be extracted at steady state ($\partial_t\mathbf{n}=0$) based on Eq. (22) to obtain

$$\tau_{\rm ad} = 0 \tag{23}$$

and

$$\tau_{\rm na} = \Big(\beta + \frac{4}{3}\frac{\lambda_{\rm H}^2}{r_0^2}\Big) b_{\rm J}. \tag{24}$$

From the perspective of dynamics, we follow standard theoretical scheme to study the dynamics of antiferromagnetic textures, we obtain the equation of motion of the Néel order parameter as

$$\tfrac{1}{\bar{a}\tilde{\gamma}}\partial_t^2\mathbf{n} + \alpha_{\rm eff}(\mathbf{r})\partial_t\mathbf{n} = \gamma\mathbf{f}_{\mathbf{n}} + \beta_{\rm eff}(\mathbf{r})b_{\rm J}\partial_x\mathbf{n}, \tag{25}$$

where $\tilde{\gamma} = \gamma/(1+\alpha^2)$, $\mathbf{f}_{\mathbf{n}}$ represents an effective field derived from the magnetic energy $E = \int d\mathbf{r}\big[\frac{\bar{a}}{2}\mathbf{m}^2 + \frac{A}{2}(\nabla\mathbf{n})^2 - \mathbf{H}\cdot\mathbf{m}\big]$ as $\mathbf{f}_{\mathbf{n}} = -\delta_{\mathbf{n}}E$, where $\mathbf{H}$ is an external magnetic field, $\bar{a}$ and A are the homogeneous and inhomogeneous exchange constants, respectively [9]. The steady state solution in the absence of external magnetic field is given as

$$v_y = 0 \quad \text{and} \quad v_x = (\beta_{\rm eff}/\alpha_{\rm eff})b_{\rm J}. \tag{26}$$

II. EFFECT OF NON-MAGNETIC IMPURITY SCATTERING ON TSHE.

An interesting aspect of antiferromagnets is that even in the adiabatic limit of smooth and slowly varying order parameter $\boldsymbol{n}(\boldsymbol{r},t)$, electrons are subjected to inter-sublattice dynamics which induces spin mistracking that can give rise to exotic spin transport with no connection to non-adiabatic processes. For example, this internal

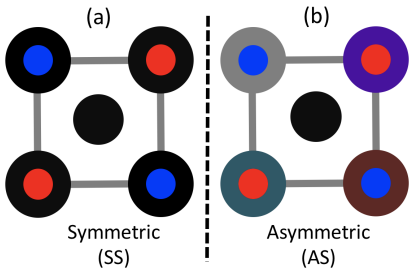

FIG. 1. Schematic illustration of the effect of (a) *SS* and (b) *AS* non-magnetic impurity scattering within an antiferromagnetic unit cell. For *SS* scattering, an interstitial defect in the unit cell introduces a symmetric (represented by the same color shield around the atoms) shift to the onsite energy while as *AS* defect result to an asymmetric (represented by different color shields around the atoms) within the unit cell.

dynamics have been shown to produce a spin-dependent renormalization of the electron's group velocity [2] equivalent to a texture-induced *intrinsic spin-orbit coupling* [3, 4]. Therefore, it is crucial to investigate effects that can influence the coherence of these inter-sub-lattice transitions such as impurity scattering that are omnipresent in real materials. We consider two classes of non-magnetic impurities defects: (i) one that preserves the coherence between the sublattices within the antiferromagnetic unit cell, referred to as *symmetric scattering (SS)*, and (ii) disorder that induces decoherence within the unit cell referred to as *asymmetric scattering (AS)*, as illustrated in Figure 1. In our model, impurities are incorporated via randomized onsite energies $\epsilon_i = \mathcal{V}_i \in \left(-\frac{W}{2}, \frac{W}{2}\right)$, where W defines the strength of the disorder, and average over 10^4 configurations to ensure convergence. First, we consider an AFM-Sk with a strong exchange energy $J = 5t$, and investigate the dependence of its Hall transport properties by means of a four-terminal system [10] on the type and strength of impurity scattering and compare with an equivalent FM-Sk. Notice that

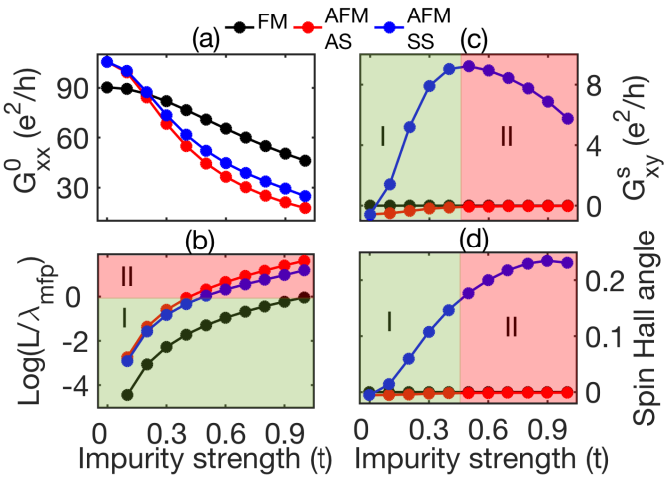

FIG. 2. Comparing the impact of impurity scattering in FM-Sks (black curve) and AFM-Sks (red and blue curves). Impurities progressively reduces the (a) longitudinal conductance in FM-Sks and AFM-SKs and hence (b) $\lambda_{\rm mfp}$ of the system.

from Eq. (2), the band width depends on the exchange strength, therefore, to avoid ambiguity associated to the position of the band gap, we place the Fermi energy at the middle of the top band i.e. $\epsilon_F = \frac{1}{2}\left(\sqrt{J^2+16}+J\right) = 5.7t$. Our numerical results as depicted in Figure 2, allows us to identify two transport regimes based on how the mean-free path of the system ($\lambda_{\rm mfp}$) compares to the system size (L). As shown in Figure 2 (b), in Region I, $\lambda_{\rm mfp} > L$ while in Region II, $\lambda_{\rm mfp} < L$. Region I represents a regime in which the *internal* (within the unit cell) dynamics of electron remains coherent. The transition from Region I into Region II represents the onset of decoherence that progressively destroys this coherent internal dynamics of electron as the impurity strength increases. Notice a close correspondence between this transition and the dependence of the spin Hall conductance on the impurity strength. Indeed, Figure 3 (c) shows that as long as the internal dynamics of electrons remains coherent, the spin Hall conductance and hence TSHE increases with increases in impurity

strength. At the onset of decoherence, the impurities destroy the coherence and the coupled sub-lattices start behaving as two independent ferromagnets resulting in a decrease in spin Hall conductance as the impurity strength increases [10]. It is worthy to note here that the enhancement of spin Hall angle (i.e. TSHE efficiency) in Figure 2 (d) as the impurity strength increases is not due to an increase in TSHE itself but due mainly to the extensive reduction in the longitudinal conductance.

We confirm the correspondence between the coherent internal dynamics of electrons and the strength of SS disorder by performing additional Hall transport calculations for different exchange strengths as a function of impurity strength and examine the relation between λ_{mfp} and the spin Hall conductance. Our results as shown in Figure 3 reveals that for $J = 0.1t$ (green curve) and $J = 0.5t$ (black curve), and for all impurity strengths considered, the disorder preserves the coherent dynamics of electrons $\lambda_{\text{mfp}} > L$ [Figure 3 (b)]. The TSHE increases with increase in impurity strength and is accompanied by a corresponding increase in both in spin Hall conductivity and topological spin Hall angle as shown in Figures 3 (c) and (d), respectively. For $J = 5.0t$ and $J = 10t$, Figure 3 (b) shows that impurity eventually drives the system from Region I into Region II as the strength of the impurity increases, with the crossover occurring around an impurity strength of $0.4t$ and $0.2t$ [blue and red curves of Figure 3 (b)], respectively . In both cases, the spin Hall conductivity and hence the TSHE increases (decreases) as the impurity strength increases below (above) the crosover [blue and red curves of Figure 3(c)].

III. MAGNETIZATION PROFILE AND USEFUL INTEGRALS

We consider an antiferromagnetic skyrmion with spin texture described by the Néel order parameter $\mathbf{n}$ given in spherical coordinates as $\mathbf{n} = (\cos\Phi\sin\theta, \sin\Phi\sin\theta, \cos\theta)$,

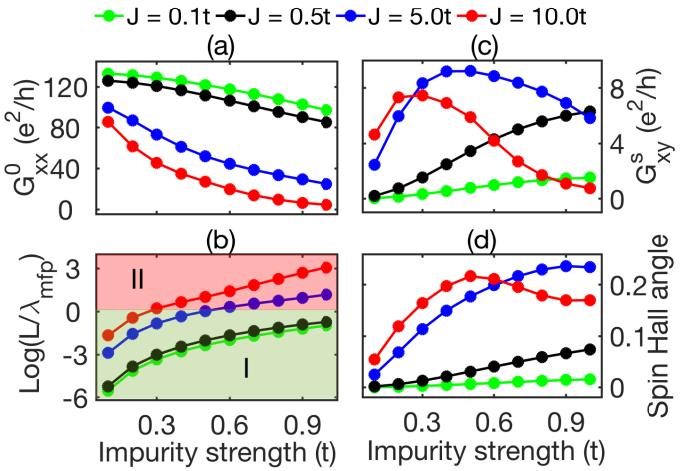

FIG. 3. Dependence of transport properties of a single AFM-Sk embedded in a system of size on the strength of *SS* impurity scattering for different exchange energies measure at the centre of the bottom band. (a) Longitudinal conductance and (b) $\lambda_{\rm mfp}$ decreases while (c) TSHE increases (for $\lambda_{\rm mfp} > L$) with increase in impurity strength. For impurity strength corresponding to $\lambda_{\rm mfp} < L$, the TSHE decreases as the impurity strength increases. (d) The efficiency of the TSHE shows enhancement with increases in impurity strength.

such that

$$\cos\theta = p\frac{r_0^2 - r^2}{r_0^2 + r^2} \quad , \quad \sin\theta = p\frac{2r_0 r}{r_0^2 + r^2} \quad \text{and} \quad \Phi = qArg(x,y) + c\frac{\pi}{2}. \tag{27}$$

r_0 is the radius of the skyrmion, while p, q, and c which take values ± 1 define the *polarity* (skyrmion core), *vorticity*, and the *chirality* of the structure, respectively. Using this profile one can straightforwardly deduce the following useful expressions:

$$\partial_x \mathbf{n} = c\frac{\sin\theta}{r}\left(p\sin\Phi\mathbf{e}_\theta + \cos\Phi\mathbf{e}_\Phi\right) \tag{28a}$$

$$\mathbf{n}\times\partial_x\mathbf{n} = pq\partial_y\mathbf{n} = c\frac{\sin\theta}{r}\left(p\sin\Phi\mathbf{e}_\Phi - \cos\Phi\mathbf{e}_\theta\right) \tag{28b}$$

$$\mathcal{N}_{x,y}(\boldsymbol{r}) = \mathbf{n}\cdot\left(\partial_x\mathbf{n}\times\partial_y\mathbf{n}\right) = pq\frac{\sin^2\theta}{r^2}, \tag{28c}$$

where $\mathbf{e}_\theta = (\cos\Phi\cos\theta, \sin\Phi\cos\theta, -\sin\theta)$ and $\mathbf{e}_\Phi = (-\sin\Phi, \cos\Phi, 0)$. For a finite system defined by a radius R, such that $R \gg r_0$, we computed the following useful integrals

$$\int_A \big(\mathbf{n}\times\partial_x\mathbf{n}\big)\cdot\big(\mathbf{n}\times\partial_x\mathbf{n}\big)\mathrm{d}^2\mathbf{r} = 4\pi\big(1-\mathcal{S}\big) \approx 4\pi, \tag{29a}$$

$$\int_A pq\mathcal{N}_{x,y}(\boldsymbol{r})\big(\mathbf{n}\times\partial_x\mathbf{n}\big)\cdot\big(\mathbf{n}\times\partial_x\mathbf{n}\big)\mathrm{d}^2\mathbf{r} = 4\pi\big(1-\mathcal{S}\big)\frac{4\mathcal{S}_2}{3r_0^2} \approx \frac{16\pi}{3r_0^2}, \tag{29b}$$

where

$$\mathcal{S} = \frac{r_0^2}{r_0^2+R^2} \quad \text{for} \quad R \gg r_0 \ , \ \mathcal{S}\to 0 \tag{30}$$

and

$$\mathcal{S}_2 = 1 + \mathcal{S} + \mathcal{S}^2 \to 1. \tag{31}$$

IV. SPIN TRANSFER TORQUE CALCULATION

We present a numerical scheme to calculate the adiabatic and non-adiabatic spin transfer torque components based on tight-binding model. We consider a large system of $302\times 302a_0^2$ containing an isolated AFM-Sk to ensure smooth magnetization variation from system to leads for all skyrmion sizes considered. This is essential as it removes unrealistic quantum oscillations of local quantities such as the non-equilibrium spin densities associated to smaller system sizes. The system is subjected to an electrical bias of $eV = 0.2t$, where $t = 1$. The local spin density at site n for electrons from the α-lead $\mathbf{S}_n^\alpha$ is computed as

$$\mathbf{S}_n^\alpha = \sum_\nu {\Psi_{n,\nu}^\alpha}^\dagger \hat{\boldsymbol{\sigma}} \Psi_{n,\nu}^\alpha, \tag{32}$$

where $\Psi_{n,\nu}^\alpha$ is the ν-mode of wave function of electrons from the α-lead at site n. From this the quantum mechanical average non-equilibrium is calculated by performing energy integration within the window $\epsilon_\mathrm{F} - \frac{eV}{2}$ to $\epsilon_\mathrm{F} + \frac{eV}{2}$ as

$$\delta\mathbf{S}_n = \sum_\alpha \int \frac{\mathrm{d}\epsilon}{2\pi}\mathbf{S}_n^\alpha f_\alpha, \tag{33}$$

where $\epsilon_{\rm F}$ is the Fermi energy and f_α is the Fermi-Dirac function for α-lead. From this, the local torque of the n-site $\mathbf{T}_n$ is straightforwardly calculated as

$$\mathbf{T}_n = (2J/\hbar)\delta\mathbf{S}_n \times \mathbf{m}_n, \tag{34}$$

where $\mathbf{m}_n$ magnetization of the n-site. From the torque the adiabatic and non-adiabatic components of the torques can be extracted by projecting on $\partial_x\mathbf{n}$ and $\mathbf{n} \times \partial_x\mathbf{n}$ respectively, and integrating over space.

---

[1] H. B. M. Saidaoui, X. Waintal, and A. Manchon, Phys. Rev. B **95**, 134424 (2017).

[2] R. Cheng and Q. Niu, Phys. Rev. B **86**, 245118 (2012).

[3] R. Cheng and Q. Niu, Phys. Rev. B **89**, 081105(R) (2014).

[4] C. A. Akosa, W.-S. Kim, A. Bisig, *et. al.*, Phys. Rev. B **91**, 094411 (2015).

[5] S. E. Barnes and S. Maekawa, Phys. Rev. Lett. **98**, 246601 (2007).

[6] Y. Tserkovnyak and M. Mecklenburg, Phys. Rev. B **77**, 134407 (2008).

[7] S. Zhang and S. S.-L. Zhang Phys. Rev. Lett. **102**, 086601 (2009).

[8] C. A. Akosa, P. B. Ndiaye, and A. Manchon, Phys. Rev. B **95**, 054434 (2017).

[9] K. M. D. Hals, Y. Tserkovnyak, and A. Brataas, Phys. Rev. Lett. **106**, 107206 (2011).

[10] P. B. Ndiaye, C. A. Akosa, and A. Manchon, Phys. Rev. B **95**, 064426 (2017).